



Article

Effect of Co Doping on Electrocatalytic Performance of Co-NiS₂/CoS₂ Heterostructures

Zehui Peng¹, Shuai Lou² , Yuan Gao¹, Lijun Kong¹, Shancheng Yan^{1,*} , Ka Wang³ and Haizeng Song³

¹ School of Geography and Biological Information, Nanjing University of Posts and Telecommunications, Nanjing 210023, China; 1019172222@njupt.edu.cn (Z.P.); 1218063835@njupt.edu.cn (Y.G.); 1020173018@njupt.edu.cn (L.K.)

² Department of Materials Science and Engineering, University of California, Berkeley, CA 94720, USA; slou@berkeley.edu

³ Collaborative Innovation Center of Advanced Microstructures, Nanjing University, Nanjing 210093, China; 1217063729@njupt.edu.cn (K.W.); DG1823028@smail.nju.edu.cn (H.S.)

* Correspondence: yansc@njupt.edu.cn

Abstract: There are abundant water resources in nature, and hydrogen production from electrolyzed water can be one of the main ways to obtain green and sustainable energy. Traditional water electrolysis uses precious metals as catalysts, but it is difficult to apply in massive volumes due to low reserves and high prices. It is still a challenge to develop hydrogen electrocatalysts with excellent performance but low cost to further improve the efficiency of hydrogen production. This article reported a potential candidate, the Co-NiS₂/CoS₂ (material is based on NiS₂, and after Co doping, The NiS₂/CoS₂ heterostructure is formed) heterostructures, prepared by hydrothermal method with carbon paper as the substrate. In a 0.5 M sulfuric acid solution, the hydrogen evolution reaction with Co-NiS₂/CoS₂ as the electrode showed excellent catalytic performance. When the Co (Cobalt) doping concentration is increased to 27%, the overpotential is −133.3 mV, which is a drop of 81 mV compared with −214.3 mV when it is not doped. The heterostructure formed after doping also has good stability. After 800 CV cycles, the difference in overpotential is only 3 mV. The significant improvement of the catalytic performance can be attributed to the significant changes in the crystal structure and properties of the doped heterostructures, which provide an effective method for efficient electrocatalytic hydrogen production.

Keywords: hydrogen evolution reaction; catalysts; heterostructures; transition metal dichalcogenides



Citation: Peng, Z.; Lou, S.; Gao, Y.; Kong, L.; Yan, S.; Wang, K.; Song, H. Effect of Co Doping on Electrocatalytic Performance of Co-NiS₂/CoS₂ Heterostructures. *Nanomaterials* **2021**, *11*, 1245. <https://doi.org/10.3390/nano11051245>

Academic Editor: Adriano Sacco

Received: 7 April 2021

Accepted: 29 April 2021

Published: 8 May 2021

Publisher's Note: MDPI stays neutral with regard to jurisdictional claims in published maps and institutional affiliations.



Copyright: © 2021 by the authors. Licensee MDPI, Basel, Switzerland. This article is an open access article distributed under the terms and conditions of the Creative Commons Attribution (CC BY) license (<https://creativecommons.org/licenses/by/4.0/>).

1. Introduction

Large scale use of pollution-free, green and sustainable energy is the future development trend [1–3]. Compared with traditional energy sources, the water produced by hydrogen combustion will not cause any pollution to the atmosphere and water resources [4–7]. At present, the common hydrogen production methods include photocatalysis and electrocatalysis, etc. [1,3]. Among them, catalysts-assisted water splitting is one of the most promising methods to generate hydrogen [8–10]. Precious metals (platinum and palladium based) are common catalysts for water splitting, and the onset potential of the Pt electrode is close to 0 mV [11]. However, due to its scarcity and high price, it is difficult to widely use in industrial hydrogen production [12–18].

Non-noble transition metal sulfides have attracted extensive attention due to their simple synthesis, low price, good stability and other advantages [19]. The transition metal sulfide catalysts with Fe, Co and Ni have the problems of insufficient active centers and low conductivity, which limit the efficiency of hydrogen production. Co doping can significantly improve the efficiency of electrocatalytic hydrogen evolution, and with the increase in Co doping, the formed heterostructures can show unique properties. Compared with NiS₂ (Nickel disulfide) nanomaterials, Co-NiS₂/CoS₂ heterostructures can promote

the rapid transfer of electrons and have strong reducibility [20–22]. Looking for the best Co doping ratio to improve the hydrogen production efficiency of transition metal sulfides is of great significance to explore green and sustainable development, but there are few studies on the influence of the Co doping ratio on the hydrogen evolution performance of transition metal sulfides.

In this paper, Co-NiS₂/CoS₂ heterostructures were prepared by the hydrothermal method, which showed good catalytic performance in 0.5 M H₂SO₄. With the increase in Co content, the catalytic activity is enhanced. When the current density is 10 mA·cm⁻², the overpotential changed from -214.3 mV to -133.3 mV with the increase in Co doping ratio, the absolute value of overpotential decreased by 81 mV, and the catalytic activity increased significantly. The relationship between the electrochemical performance and chemical characterization of Co-NiS₂/CoS₂ heterostructures with different doping concentrations was explored to find the best doping ratio. Doping a certain proportion of non-noble metal catalyst is an effective way to improve the efficiency of electro catalytic hydrogen production, which is expected to solve the problems of the high cost of traditional noble metal electro catalytic hydrogen production and the low efficiency of non-noble metal hydrogen production.

2. Materials and Methods

2.1. Materials and Chemicals

SC(NH₂)₂, NiSO₄·6H₂O used in the experiment was purchased from Shanghai Titan Technology Co., Ltd. (Shanghai, China). Sulfur powder (S) was obtained from Nanjing Chemical Reagent Co., Ltd. (Nanjing, China). Co(NO₃)₂·6H₂O used in the experiment was purchased from Shanghai Aladdin Biochemical Technology Co., Ltd. (Shanghai, China), while H₂SO₄ and C₂H₅OH were acquired from Shanghai Titan Technology Co., Ltd. (Shanghai, China).

2.2. Synthesis of Co-NiS₂/CoS₂ Heterostructures

The preparation of Co-NiS₂/CoS₂ heterostructures is shown in Figure 1a. Take the preparation of Co-NiS₂/CoS₂ heterostructures with 27% Co doping ratio as an example: the carbon paper (2 cm × 2 cm) is washed with deionized water and ethanol for 15 min, respectively. Co(NO₃)₂·6H₂O (0.324 mM), NiSO₄·6H₂O (1.2 mM), SC (NH₂)₂ (1.8 mM) and 25 mL deionized water are added to 50 mL polytetrafluoroethylene reactor. The reactor is placed on a magnetic stirrer and stirred at a high speed for 15 min to form a uniform and transparent solution. Then, the 0.96 mM sulfur powder is slowly poured into the above reactor during the stirring process, the stirring speed is reduced, and the stirring is continued for 10 min. After the stirring is stopped, the sulfur powder forms a film on the solution. Then, the clean carbon paper is stuck vertically in the reactor, the carbon paper needs to be completely immersed in the solution, and then the reactor is tightened and placed in the 180 °C blast furnace for 8 h. After the reaction, the Co-NiS₂/CoS₂ heterostructures condensed on the surface of carbon paper were taken out of the reactor together with carbon paper, and washed twice with alcohol and deionized water. Finally, the residual deionized water on the surface is blown dry with a hot air blower.

2.3. Materials Characterization

The crystals Co-NiS₂/CoS₂ was analyzed by X-ray diffractometer (XRD) (Bruker Daltonics Inc., Karlsruhe, Germany). The micromorphology of the heterojunction was obtained by scanning electron microscope (FE-SEM; JSM-7000F JEOL Ltd., Tokyo, Japan). Transmission electron microscope (TEM) and Energy dispersive X-ray (EDXA) were taken by JEOL type JEM2100 instrument (JEOL Ltd., Tokyo, Japan). The chemical structure and element valence state of heterostructures were analyzed by X-ray electron spectrometry (XPS, PHI5000 Versaprobe Ulvac-Phi Inc., Kanagawa, Japan). Raman measurements by Horiba LabRAM system (HORIBA, Ltd., Kyoto, Japan).

2.4. Electrochemical Measurements

The CHI760E electrochemical analyzer (CH Instruments, Chenhua Co., Shanghai, China) was used to analyze the performance of samples. The test uses a three-electrode system with the sample, platinum and saturated calomel electrode as the working electrode (the loading of the catalyst on the carbon paper, about 11 mg), counter electrode and reference electrode, respectively.

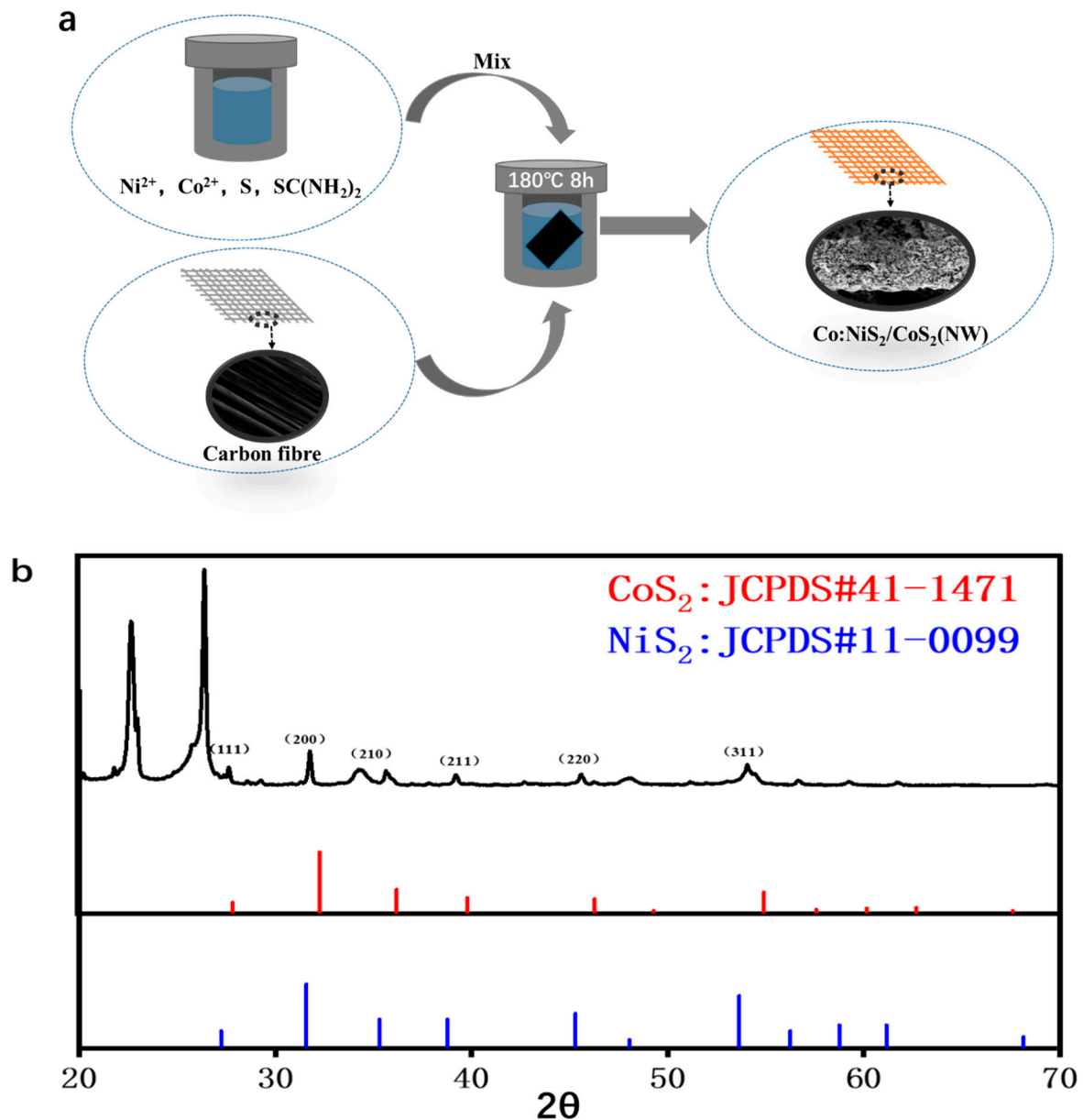


Figure 1. (a) Flow chart of hydrothermal preparation of $\text{Co-NiS}_2/\text{CoS}_2$ heterostructures; (b) XRD pattern of $\text{Co-NiS}_2/\text{CoS}_2$ heterostructures doped with 27% Co.

3. Results and Discussion

In order to further study the crystal structure of the samples, we measured the X-ray diffraction (XRD). The XRD patterns of $\text{Co-NiS}_2/\text{CoS}_2$ are shown in Figure 1b. The diffraction peaks at $2\theta = 27.2^\circ, 31.6^\circ, 35.3^\circ, 38.8^\circ, 45.3^\circ$ and 53.6° can be aligned to the NiS_2 (JCPDS#11-0099) plane at (111), (200), (210), (211), (220), (311) [22–24]. There are also some peaks corresponding to CoS_2 (JCPDS#41-1471) [25–27], and bare carbon fiber shows peak

located at 26.4° [28]. Compared with pure NiS_2 , these peak positions are shifted by 0.04° after Co doping, which indicates that Co is doped into the NiS_2 phase [29].

As shown in Figure 2a and Supplementary Figure S4, undoped pure NiS_2 nanomaterial shows regular crystal structure and smooth surface. With the increase in Co doping concentration, the regular crystal structure changes to a coral flower shape, and the wheat spike structure can be observed in the further enlarged image, which is conducive to the exposure of the catalytic active centers, thereby improving the catalytic efficiency [30,31]. When the Co content reaches up to 27%, the $\text{Co-NiS}_2/\text{CoS}_2$ heterostructures has the largest catalytic active region and the best electrocatalytic performance. As shown in Figure 2b, the $\text{Co-NiS}_2/\text{CoS}_2$ heterostructures presents a linear structure. Figure 2c is the HRTEM image of 27% Co doped $\text{Co-NiS}_2/\text{CoS}_2$ heterostructures. Obvious crystal segmentation lines were observed, forming ordered $\text{Co-NiS}_2/\text{CoS}_2$ heterostructures. The lattice constants of CoS_2 and NiS_2 are 0.248 nm (210) and 0.254 nm (210), respectively [26,31,32]. Figure 2e–g show EDXA (Energy dispersive X-ray) elemental mapping of Ni, Co and S, respectively. Additionally, the energy dispersive X-ray elemental mapping further reveals that the CoS_2 nanosheet was successfully attached to the NiS_2 nanosheet, forming a highly exposed interface [33].

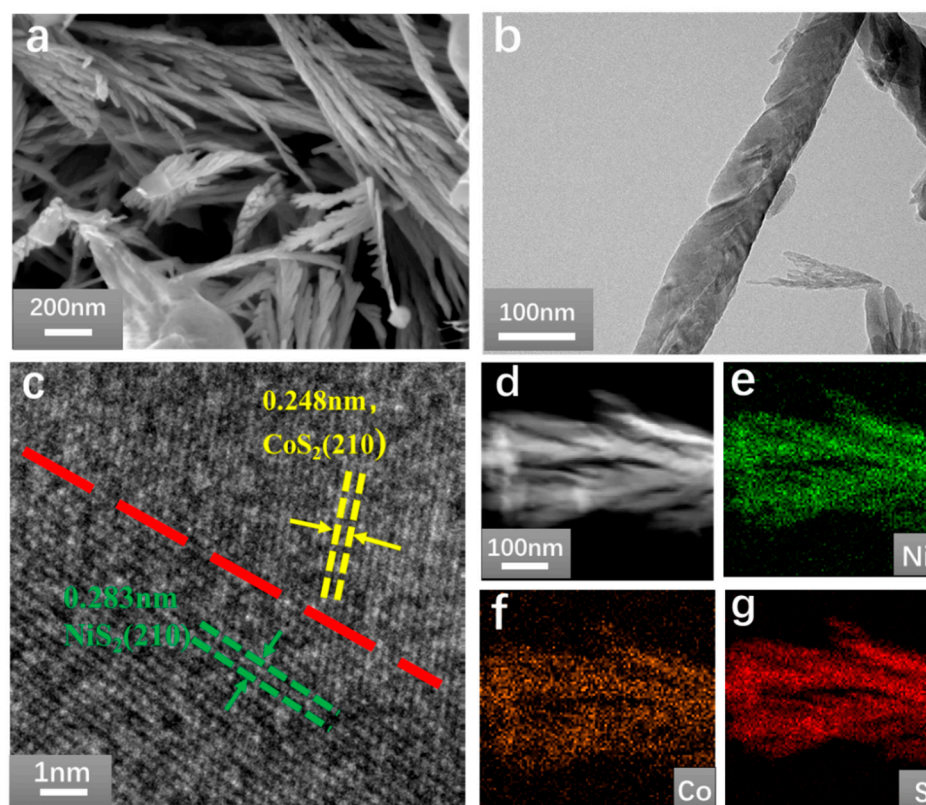


Figure 2. (a) SEM images of $\text{Co-NiS}_2/\text{CoS}_2$ heterostructures; (b) TEM image of $\text{Co-NiS}_2/\text{CoS}_2$ heterostructures; (c) HRTEM image of $\text{Co-NiS}_2/\text{CoS}_2$ heterostructures; (d–g) STEM image and EDXA elemental mapping of Ni, Co, and S for $\text{Co-NiS}_2/\text{CoS}_2$ heterostructures.

By means of EDXA and XPS (X-ray photoelectron spectroscopy), the chemical composition and valence state of $\text{Co-NiS}_2/\text{CoS}_2$ were further understood. Figure 3a shows the complete XPS spectrum of 27% $\text{Co-NiS}_2/\text{CoS}_2$ heterostructures. The peaks observed at 854.2 eV and 855.7 eV are attributed to $\text{Ni}2p_{3/2}$ and $\text{Ni}2p_{1/2}$ of Ni^{2+} , respectively, and the peaks at 871.9 eV and 875.5 eV are attributed to $\text{Ni}2p_{3/2}$ and $\text{Ni}2p_{1/2}$ of Ni^{3+} , respectively. The existence of NiS_2 was further confirmed by the peaks of Ni^{2+} and Ni^{3+} and the satellite peaks of 861.7 eV and 879.6 eV (Figure 3b) [34,35]. As the XPS spectrum of Co is shown in Figure 3c. The Co 2p spectrum was deconvoluted to three spin-orbit doublets. The peaks

at binding energies of 778.9 and 793.6 eV were assigned to Co of Co: NiS₂, and those at 771.6 and 796.1 eV originated from Co:CoS₂. Two shake-up satellites corresponding to oxidized Co species of Co: NiS₂/CoS₂ were also observed [33,36,37]. The peaks of S2p_{3/2} and S2p_{1/2} were observed at about 162.5 eV and 163.7 eV, respectively. Due to slight surface oxidation, the weak peak at approximately 168 eV can be identified as an S-O bond (Figure 3d) [31,38].

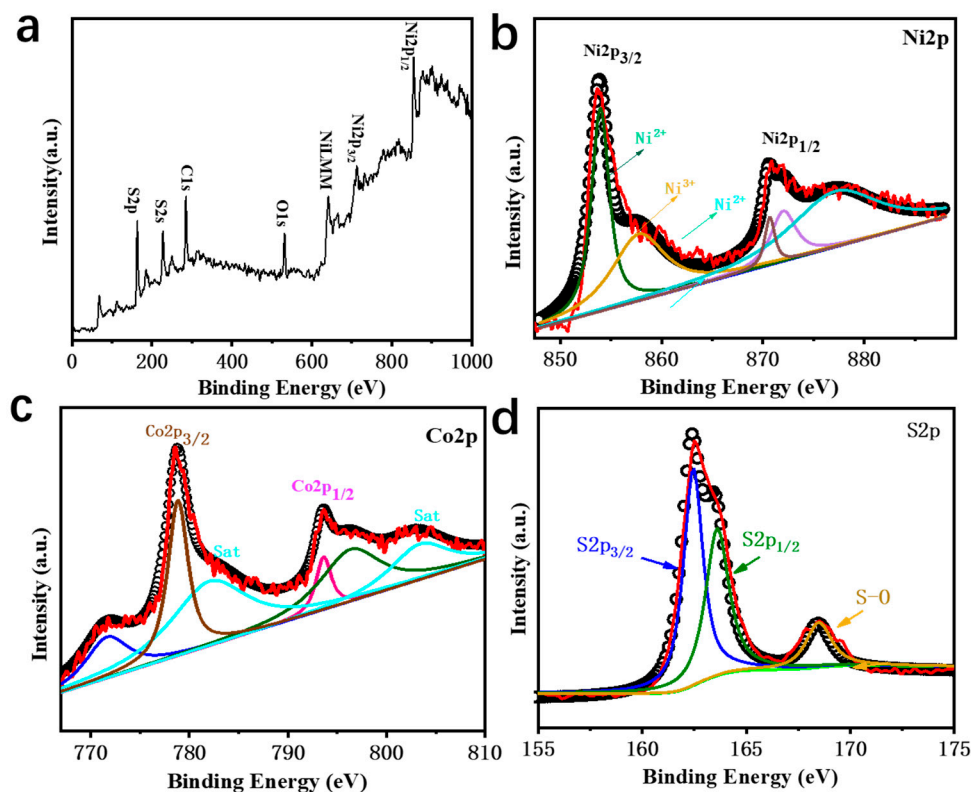


Figure 3. (a) Survey spectrum, and high-resolution; (b) Ni 2p; (c) Co 2p spectrum; (d) S 2p spectrum.

Yang et al. [39] reported one 3D hybrid of CoSe nanoparticles encapsulated nitrogen-doped carbon nanotubes graft onto nitrogen-doped carbon nanosheets (denoted as CoSe@NCNT/NCN) prepared by a one-step method. Its overpotential in the 0.5 M H₂SO₄ solution is 197 mV, and the Tafel slope is 43 mV·dec⁻¹. The electrode we prepared is based on NiS₂. After Co doping; the catalytic performance of the formed NiS₂/CoS₂ heterostructure has been significantly improved as the amount of Co doped increases. In our experiment, we tested linear sweep voltammetry (LSV) to study the catalytic efficiency of Co-NiS₂/CoS₂ heterostructures with different Co doping ratio. The Co doping ratios in the heterostructures by precise weighing are 0%, 2%, 6%, 13%, 20% and 27%, respectively. As shown in Figure 4a, as the proportion of Co doping increases, the overpotential is −214.3, −173.3, −174, −162.3, −144.3 and −133.3 mV, respectively. In order to compare with the hydrogen evolution of precious metals, we further tested the LSV curve of the Pt electrode, and the overpotential of Pt was about −26.8 mV. With the increase in the Co doping concentration, the overpotential of 214.3 mV for undoped Co changes to 133.3 mV when the Co doping ratio is 27%. The absolute value of the overpotential is significantly reduced by about 40%, and the hydrogen evolution catalytic performance is significantly enhanced. As shown in Figure 4b, it can be observed that with the increase in Co doping concentration, the Tafel slope presents a downward trend, and the slope is nearly doubled (0% Co-240 mV·dec⁻¹, 27% Co-123 mV·dec⁻¹). By testing the electrochemical performance of 27% Co doped sample after 800 CV cycles, the absolute value of overpotential is only 3 mV different from that before cycling, indicating that the sample has good stability (Figure 4d). Through the experimental data, we found that when the Co doping concentration is 27%,

the absolute value of overpotential is the smallest, the hydrogen evolution performance is the best, and it also has good stability. As shown in Figure S1, when Co is not doped or the doping concentration is low, the Raman spectrum has two higher peaks at 270 cm^{-1} and 480 cm^{-1} [40,41]. With the increase in doping concentration, especially 27% Co doping, the heterostructures is formed, the peak width increases and the crystallinity decreases. This is further confirmed by the scanning electron microscopy (SEM) images of each Co doping concentration in Figure S4. When the initial state of Co is not doped, the SEM spectrum is angular crystal structure, and the crystal is evenly distributed on the carbon fiber tube. When the proportion of Co doping increases, flowerlike particles appear on the regular crystal. When the proportion of Co doping reaches 27%, the regular crystal basically disappears, and only irregular coral flowerlike structure can be seen on the carbon fiber.

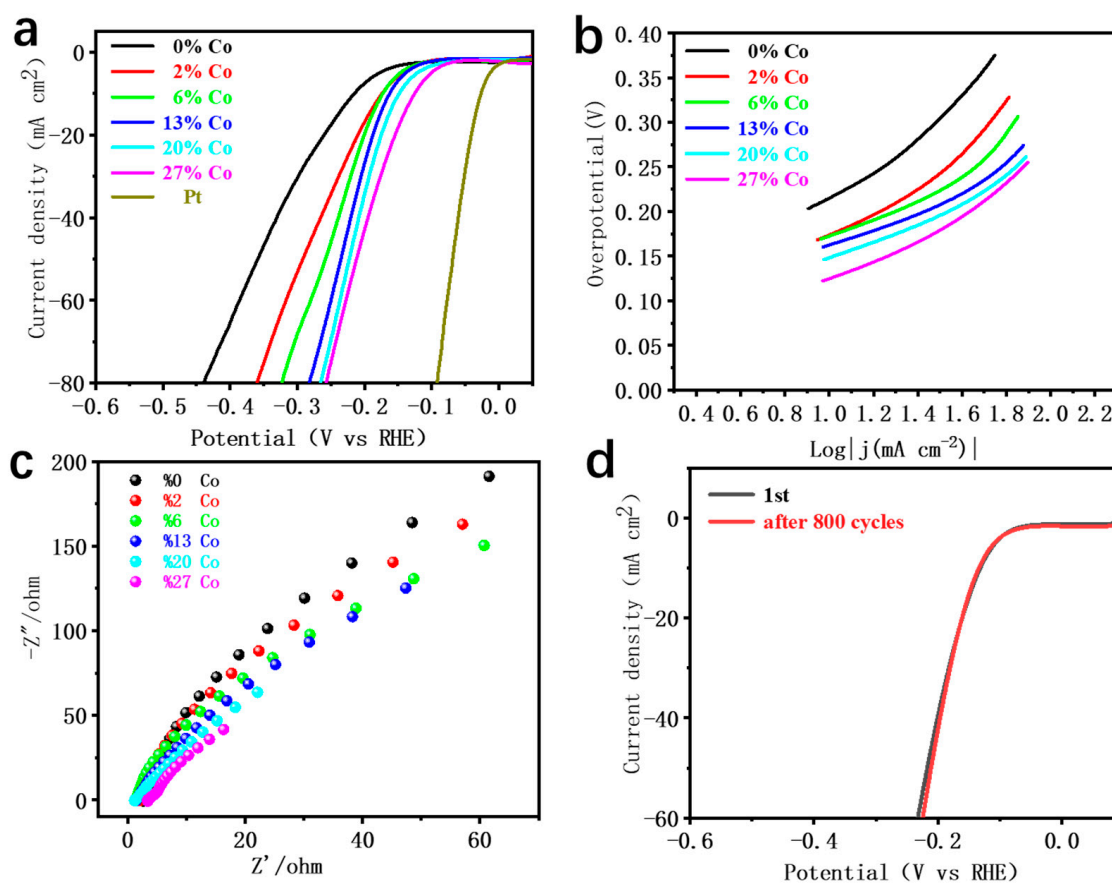


Figure 4. (a) LSV curves of Co-NiS₂/CoS₂ heterostructures with different Co doping concentrations in H₂SO₄ solution; (b) Tafel curves of Co-NiS₂/CoS₂ heterostructures with different Co doping concentrations in H₂SO₄ solution; (c) electrochemical impedance spectroscopy of samples; (d) LSV curves before and after 800 CV cycles.

As shown in Figures S2a and S3a, in order to analyze the activity difference between Co-NiS₂/CoS₂ heterostructures and undoped NiS₂, we measured different scanning rates (5, 10, 20, 30, 40, 50, 60, 70, 80, 90 and 100) by cyclic voltammetry (CV). As shown in Figures S2b and S3b, the electrochemical surface area (ECSA) of undoped and 27% doped Faraday double-layer capacitor (Cdl) is obtained. The catalytic performance of the working electrode is normalized to 1 cm^{-2} [24,42,43]. We applied the specific capacitance ($20\text{--}60\text{ }\mu\text{F cm}^{-2}$) of $40\text{ }\mu\text{F cm}^{-2}$ here to calculate the ECSA [4]. The surface active area of the doped catalytic material is about 0.72 cm^{-2} , and the surface active area of pure NiS₂ is 0.61 cm^{-2} . The calculated results show that the catalytic activity of the electrode doped with 27% Co is stronger, which indicates that the catalytic activity of the electrode doped with Co is enhanced. Figure 4c is the electrochemical impedance spectroscopy (EIS) diagram of the different doping concentrations. Further experimental studies show

that with the increase in the Co doping ratio (34%), the structure and properties of the heterostructures are not significantly different from that of the heterostructures doped with 27%. As the amount of Co doping continues to increase, the surface of the catalyst is covered with a large number of particles, the nanowires are reduced, and the active area of the catalyst is reduced. A high proportion of Co doping cannot achieve a better doping income. The results show that with the increase in Co doping in a certain range, high doping concentration has better conductivity, and the catalytic performance is also improved compared with low doping concentration.

4. Conclusions

To sum up, we prepared Co doped nanowires with different Co concentrations by hydrothermal method Co-NiS₂/CoS₂ heterostructures, and through experimental verification we found that Co doping can greatly improve the efficiency of transition metal sulfide electrocatalytic hydrogen production. At the same time, we found that the best catalytic efficiency is achieved when the doping concentration is 27%, which is expected to solve the problem of high cost and difficult large-scale industrial production of traditional noble metal catalytic hydrogen production, and provide a practical idea and method for large-scale production of hydrogen clean energy.

Supplementary Materials: The following are available online at <https://www.mdpi.com/article/10.3390/nano11051245/s1>, Figure S1: Raman spectra of Co doped Co-NiS₂/CoS₂ heterostructures with a-f ratios of 0%, 2%, 6%, 13%, 20% and 27%, respectively; Figure S2: (a) Cyclic voltammograms of 27% Co doped Co-NiS₂/CoS₂ heterostructures at different scan rates; (b) Calculation of the relationship between scanning rate and 27% Co doped Co-NiS₂/CoS₂ heterostructures in double-layer capacitor by linear fitting of capacitive current; Figure S3: (a) Cyclic voltammograms of 0% Co doped Co-NiS₂/CoS₂ heterostructures at different scan rates; (b) Calculation of the relationship between scanning rate and 0% Co doped Co-NiS₂/CoS₂ heterostructures in double-layer capacitor by linear fitting of capacitive current; Figure S4: SEM spectra of Co doped Co-NiS₂/CoS₂ heterostructures with a-f ratio of 0%, 2%, 6%, 13%, 20% and 27%, respectively; Table S1. The comparison of electrocatalytic performance of the latest and related research.

Author Contributions: Conceptualization, S.Y. and K.W.; methodology, Z.P. and Y.G.; validation, Z.P. and L.K.; investigation, S.L. and Z.P.; data curation, Z.P. and Y.G.; writing—original draft preparation, Y.G. and Z.P.; writing—review and editing, S.Y.; supervision, S.L.; project administration, S.Y.; funding acquisition, S.Y.; TEM test, H.S.; XRD test, H.S. All authors have read and agreed to the published version of the manuscript.

Funding: This work is supported by the National Science Foundation of China (No. 61991431, No. 11574136), the National Basic Research Program of China (2018YFA0209101).

Data Availability Statement: Data is contained within the article or Supplementary Materials.

Conflicts of Interest: The authors declare no competing financial interest.

References

1. Lim, Y.; Lee, D.-K.; Kim, S.M.; Park, W.; Cho, S.Y.; Sim, U. Low Dimensional Carbon-Based Catalysts for Efficient Photocatalytic and Photo/Electrochemical Water Splitting Reactions. *Materials* **2019**, *13*, 114. [CrossRef]
2. Rusinque, B.; Escobedo, S.; Lasa, H.D. Hydrogen Production via Pd-TiO₂ Photocatalytic Water Splitting under Near-UV and Visible Light: Analysis of the Reaction Mechanism. *Catalysts* **2021**, *11*, 405–430. [CrossRef]
3. Tang, C.; Gan, L.F.; Zhang, R.; Lu, W.B.; Jiang, X. Ternary Fe_xCo_{1-x}P nanowire array as a robust hydrogen evolution reaction electrocatalyst with Pt-like activity: Experimental and theoretical insight. *Nano Lett.* **2016**, *16*, 6617–6621. [CrossRef] [PubMed]
4. Zhou, G.; Shan, Y.; Wang, L.; Hu, Y.; Guo, J.; Hu, F. Photoinduced semiconductor-metal transition in ultrathin troilite fes nanosheets to trigger efficient hydrogen evolution. *Nat. Commun.* **2019**, *10*, 399–407. [CrossRef]
5. Ayala, P.; Giesriegl, A.; Nandan, S.P.; Myakala, S.N.; Cherevan, A.S. Supplementary information_isolation strategy towards earth-abundant single-site co-catalysts for photocatalytic hydrogen evolution reaction. *Catalysts* **2021**, *11*, 417–436. [CrossRef]
6. Momirlan, M.; Veziroglu, T.N. Current status of hydrogen energy. *Renew. Sustain. Energy Rev.* **2002**, *6*, 141–179. [CrossRef]
7. Wang, J.; Cui, W.; Liu, Q.; Xing, Z.; Asiri, A.M.; Sun, X. Recent progress in cobalt-based heterogeneous catalysts for electrochemical water splitting. *Adv. Mater.* **2016**, *28*, 215–230. [CrossRef] [PubMed]

8. Cronin, L.; Lie, J.; Yang, J.J.; Liu, T.; Yuan, R.M.; Deng, D.R. Tuning redox active polyoxometalates for efficient electron-coupled proton-buffer-mediated water splitting. *Chem. A Eur. J.* **2019**, *25*, 11432–11436. [[CrossRef](#)]
9. Shi, X.; Qian, Y.; Yang, S. Fluctuation Analysis of a Complementary Wind–Solar Energy System and Integration for Large Scale Hydrogen Production. *ACS Sustain. Chem. Eng.* **2020**, *8*, 7097–7110. [[CrossRef](#)]
10. Zhu, J.; Ni, Y. Phase-controlled synthesis and the phase-dependent HER and OER performances of nickel selenide nanosheets by an electrochemical deposition route. *Cryst. Eng. Commun.* **2018**, *20*, 3344–3352. [[CrossRef](#)]
11. Tian, J.; Qian, L.; Asiri, A.M.; Sun, X. Self-supported nanoporous cobalt phosphide nanowire arrays: An efficient 3d hydrogen-evolving cathode over the wide range of pH 0–14. *J. Am. Chem. Soc.* **2014**, *136*, 7587–7590. [[CrossRef](#)] [[PubMed](#)]
12. Ma, R.G.; Zhou, Y.; Chen, Y.F.; Li, P.X.; Liu, Q. Ultrafine molybdenum carbide nanoparticles composited with carbon as a highly active hydrogen-evolution electrocatalyst. *Angew. Chem.* **2015**, *54*, 14723–14727. [[CrossRef](#)] [[PubMed](#)]
13. Wang, D.Y.; Gong, M.; Chou, H.L.; Pan, C.J.; Chen, H.A. Highly active and stable hybrid catalyst of cobalt-doped FeS₂ nanosheets–carbon nanotubes for hydrogen evolution reaction. *J. Am. Chem. Soc.* **2015**, *137*, 1587–1592. [[CrossRef](#)]
14. Faber, M.S.; Lukowski, M.A.; Ding, Q.; Kaiser, N.S.; Jin, S. Earth-abundant metal pyrites (FeS₂, CoS₂, NiS₂, and their alloys) for highly efficient hydrogen evolution and polysulfide reduction electrocatalysis. *J. Phys. Chem. C* **2014**, *118*, 21347–21356. [[CrossRef](#)]
15. Zou, X.; Zhang, Y. Cheminform abstract: Noble metal-free hydrogen evolution catalysts for water splitting. *Chem. Soc. Rev.* **2015**, *46*, 5148–5180. [[CrossRef](#)] [[PubMed](#)]
16. Yin, J.; Li, Y.X.; Lv, F.; Lu, M.; Sun, K. Oxygen vacancies dominated NiS₂/CoS₂ interface porous nanowires for portable Zn-air batteries driven water splitting devices. *Adv. Mater.* **2017**, *29*, 1704681. [[CrossRef](#)] [[PubMed](#)]
17. Jasion, D.; Barforoush, J.M.; Qiao, Q.; Zhu, Y.; Ren, S.; Leonard, K.C. Low-dimensional hyperthin FeS₂ nanostructures for efficient and stable hydrogen evolution electrocatalysis. *ACS Catal.* **2015**, *5*, 6653–6657. [[CrossRef](#)]
18. Wu, T.; Pi, M.; Wang, X. Three-dimensional metal–organic framework derived porous CoP₃ concave polyhedrons as superior bifunctional electrocatalysts for the evolution of hydrogen and oxygen. *Phys. Chem. Chem. Phys.* **2017**, *19*, 2104–2110. [[CrossRef](#)] [[PubMed](#)]
19. Wang, Y.; Wang, Q.; Zhan, X.; Wang, F.M.; Safdar, J.H. Visible light driven type II heterostructures and their enhanced photocatalysis properties: A review. *Nanoscale* **2013**, *5*, 8326–8339. [[CrossRef](#)]
20. Wang, L.H.; Zhang, Z.; Chen, J.; Hu, S.; Li, Z.; Wang, J.; Liu, X.; Wang, C. Semiconductor heterojunction photocatalysts: Design, construction, and photocatalytic performances. *Soc. Rev.* **2014**, *43*, 5234–5244. [[CrossRef](#)]
21. Jang, J.S.; Kim, H.G.; Lee, J.S. Heterojunction semiconductors: A strategy to develop efficient photocatalytic materials for visible light water splitting. *Catal. Today* **2012**, *185*, 270–277. [[CrossRef](#)]
22. Wang, W.; Li, L.; Tan, S.; Wu, K.; Zhu, G.; Liu, Y. Preparation of NiS₂/MoS₂ catalysts by two-step hydrothermal method and their enhanced activity for hydrodeoxygenation of p-cresol. *Fuel* **2016**, *179*, 1–9. [[CrossRef](#)]
23. Akbarzadeh, R.; Dehghani, H.; Behnoudnia, F. Sodium thiosulfate-assisted synthesis of NiS₂ nanostructure by using nickel(II)-Salen precursor: Optical and magnetic properties. *Dalton Trans.* **2014**, *43*, 16745–16753. [[CrossRef](#)] [[PubMed](#)]
24. Tang, C.; Pu, Z.; Liu, Q.; Asiri, A.M.; Sun, X. NiS₂ nanosheets array grown on carbon cloth as an efficient 3d hydrogen evolution cathode. *Electrochim. Acta* **2015**, *153*, 508–514. [[CrossRef](#)]
25. Senthil, R.A.; Wang, Y.; Osman, S.; Pan, J.; Lin, Y.; Shu, X. A facile one-pot synthesis of microspherical-shaped CoS₂/CNT composite as Pt-free electrocatalyst for efficient hydrogen evolution reaction. *Int. J. Hydrogen Energy* **2019**, *44*, 16537–16547. [[CrossRef](#)]
26. Sun, P.; Yan, M.G.; Zhang, H.Z.; Huang, Q.; Liu, P.L. Detection of heavy metal ions by differential pulse stripping voltammetry. *J. Univ. Electron. Technol. China* **2017**, *46*, 784–789. [[CrossRef](#)]
27. Xia, Z.D. In situ synthesis of CoS₂/rGO nanocomposites with enhanced electrode performance for lithium-ion batteries. *J. Alloys Compd.* **2013**, *579*, 372–376. [[CrossRef](#)]
28. Hao, J.; Yang, W.; Hou, J.; Mao, B.; Huang, Z.; Shi, W. Nitrogen doped NiS₂ nanoarrays with enhanced electrocatalytic activity for water oxidation. *J. Mater. Chem. A* **2017**, *5*, 17811–17816. [[CrossRef](#)]
29. An, S.; Wang, K.; Zhou, F.; Lin, S.; Song, H.; Shi, Y.; Yao, J. Ultrafine Co:FeS₂/CoS₂ Heterostructure Nanowires for Highly Efficient Hydrogen Evolution Reaction. *ACS Appl. Energy Mater.* **2019**, *3*, 514–520. [[CrossRef](#)]
30. Jung, C.T.; Hon, M.-H.; Leu, I.-C. Fabrication of mesoporous CoS₂ nanotube arrays as the counter electrodes of dye-sensitized solar cells. *Chem. Asian J.* **2015**, *10*, 1932–1939. [[CrossRef](#)]
31. Nesbitt, H.W.; Legrand, D.; Bancroft, G.M. Interpretation of Ni2p XPS spectra of Ni conductors and Ni insulators. *Phys. Chem. Miner.* **2000**, *27*, 357–366. [[CrossRef](#)]
32. Marini, C.; Joseph, B.; Caramazza, S.; Capitani, F.; Bendele, M.; Mitrano, M. Local disorder investigation in NiS₂-xSe_x using Raman and Ni K-edge x-ray absorption spectroscopies. *J. Phys. Condens. Matter.* **2014**, *26*, 452201. [[CrossRef](#)]
33. Ouyang, C.; Feng, S.; Huo, J.; Wang, S. Three-dimensional hierarchical MoS₂/CoS₂ heterostructure arrays for highly efficient electrocatalytic hydrogen evolution. *Green Energy Environ.* **2017**, *2*, 134–141. [[CrossRef](#)]
34. Dai, Y.; Niu, L.; Zou, J.; Chen, T.; Liu, H.; Zhou, Y. Preparation of core-shell magnetic Fe₃O₄/SiO₂-dithiocarbamate nanoparticle and its application for the Ni²⁺, Cu²⁺ removal. *Chin. Chem. Lett.* **2018**, *29*, 887–891. [[CrossRef](#)]
35. Gao, N.; Li, W.-P.; Wang, W.-S.; Liu, D.-P.; Cui, Y.-M.; Guo, L.; Wang, G.-S. Balancing Dielectric Loss and Magnetic Loss in Fe–NiS₂/NiS/PVDF Composites toward Strong Microwave Reflection Loss. *ACS Appl. Mater. Interfaces* **2020**, *12*, 14416–14424. [[CrossRef](#)]

36. Wang, L.; Zhang, X.; Ma, Y.; Yang, M.; Qi, Y. Supercapacitor Performances of the MoS₂/CoS₂ Nanotube Arrays in Situ Grown on Ti Plate. *J. Phys. Chem. C* **2017**, *121*, 9089–9095. [[CrossRef](#)]
37. Zhao, W.-W.; Bothra, P.; Lu, Z.; Li, Y.; Mei, L.-P.; Liu, K.; Zhao, Z.; Chen, G.; Back, S.; Siahrostami, S.; et al. Improved Oxygen Reduction Reaction Activity of Nanostructured CoS₂ through Electrochemical Tuning. *ACS Appl. Energy Mater.* **2019**, *2*, 8605–8614. [[CrossRef](#)]
38. Liu, H.; Hengjie, L.; Jiang, H.; Lin, Y.; Zhang, Y.; Habib, M.; Chen, S.; Song, L. Electronic Structure Reconfiguration toward Pyrite NiS₂ via Engineered Heteroatom Defect Boosting Overall Water Splitting. *ACS Nano* **2017**, *11*, 11574–11583. [[CrossRef](#)] [[PubMed](#)]
39. Yang, M.; Yang, Y.; Wang, K.; Li, S.; Feng, F.; Lan, K.; Jiang, P.; Huang, X.; Yang, H.; Li, R. Facile synthesis of CoSe nanoparticles encapsulated in N-doped carbon nanotubes-grafted N-doped carbon nanosheets for water splitting. *Electrochim. Acta* **2020**, *337*, 135685. [[CrossRef](#)]
40. Lyapin, S.G.; Utyuzh, A.N.; Petrova, A.E.; Novikov, A.P.; Lograsso, T.A.; Stishov, S.M. Raman studies of nearly half-metallic ferromagnetic CoS₂. *J. Physics Condens. Matter* **2014**, *26*, 396001. [[CrossRef](#)]
41. Soofivand, F.; Esmaili, E.; Sabet, M.; Salavati-Niasari, M. Simple synthesis, characterization and investigation of photocatalytic activity of NiS₂ nanoparticles using new precursors by hydrothermal method. *J. Mater. Sci. Mater. Electron.* **2018**, *29*, 858–865. [[CrossRef](#)]
42. Faber, M.S.; Dziejcz, R.; Lukowski, M.A.; Kaiser, N.S.; Ding, Q.; Jin, S. High-Performance Electrocatalysis Using Metallic Cobalt Pyrite (CoS₂) Micro-and Nanostructures. *J. Am. Chem. Soc.* **2014**, *136*, 10053–10061. [[CrossRef](#)] [[PubMed](#)]
43. Wang, K.; Guo, W.; Yan, S.; Song, H.; Shi, Y. Hierarchical Co–FeS₂/CoS₂ heterostructures as a superior bifunctional electrocatalyst. *RSC Adv.* **2018**, *8*, 28684–28691. [[CrossRef](#)]